Energy Conversion and Management: X 20 (2023) 100432

Contents lists available at ScienceDirect

Energy Conversion and Management: X

journal homepage: www.sciencedirect.com/journal/energy-conversion-and-management-x

Assessment of the Trilateral Flash Cycle potential for efficient solar energy conversion in Europe

Anastasios Skiadopoulos [a,*], Christina Antonopoulou [b], Konstantinos Atsonios [b], Panagiotis Grammelis [b], Apostolos Gkountas [c], Panteleimon Bakalis [c], Dimitrios Manolakos [a]

[a] Agricultural University of Athens, Dept. of Natural Resources Management and Agricultural Engineering, Athens, Greece
[b] Centre of Research and Technology Hellas, Chemical Process & Energy Resources Institute, Athens, Greece
[c] Psyctotherm SME, Piraeus, Greece

ARTICLE INFO

Keywords:
Solar-trilateral flash cycle
Two-phase expansion
Solar efficiency
Thermal efficiency
Exergy efficiency
Economics

ABSTRACT

The potential of the Trilateral Flash Cycle (TFC) for the efficient conversion of solar energy to power in Europe is assessed in this work. A numerical analysis of a Solar-TFC thermal power unit is performed, by applying an in-house numerical model. Flat Plate Collectors (FPC) and Evacuated Tube Collectors (ETC) are modeled as solar heat sources. Particular focus is on the technological bottleneck of the TFC, i.e. two-phase expansion, by applying a novel two-phase expansion numerical model. Annual simulations are performed with the total efficiency of the Solar-TFC maximized at each time step. The annual total efficiency of the Solar-TFC, exergy efficiency, and thermal efficiency of the TFC can be as high as 5%, 5.3%, and 11%, respectively. ETCs increase the economic viability of the Solar-TFC, particularly as the annual electricity output increases. The Levelized Cost of Electricity (LCOE) of the modeled unit is estimated in the range of 0.25 and 0.75 €/kWh, which can be further reduced by increasing the collectors' area. The Solar-TFC unit can reduce, on an annual basis, the CO_2 emissions by 2.5–47 kg per m^2 of solar collectors, with the carbon footprint reduction depending on the collectors' efficiency and the installation location.

1. Introduction

Climate change, along with the ever-increasing global energy demand, has led to the formation of policies for an environmentally friendly and efficient transition of energy systems. The European Union has the ambition to become the first climate-neutral economy by 2050 [1], and the European Commission identifies electricity as the energy type that will play the most significant role in the transition to a carbon-free energy system [2]. The exploitation of renewable energy sources will significantly reduce the carbon footprint of electric power systems. However, the applicability of new technologies for the decarbonization of electric power systems must be assessed based on their sustainability. Therefore, additional factors, including overall efficiency, lifetime environmental footprint, and economics, must be taken into consideration.

Solar energy is going to play a significant role in the transition of energy systems because it is ideal for decentralized electricity production which increases significantly the primary energy conversion efficiency. Moreover, solar technology has key advantages, such as its modularity and low maintenance cost, that are anticipated to further enhance its penetration in the energy mix. Photovoltaics and solar thermal collectors are utilized to transform solar irradiance into electricity. Solar thermal collectors harvest solar irradiance and generate heat that can be exploited by a power-producing technology in solar thermal power units. Different types of solar thermal collectors, with different ranges of applications, have been developed [3] and they are currently at a mature technological level [4]. These collectors provide low-temperature heat, typically at temperatures lower than 400 °C, where the traditional water-steam Rankine power cycles of central power stations cannot operate efficiently [5–7].

The total efficiency of solar thermal power units depends on two factors, i.e. the collectors' solar harvesting efficiency and the achievable heat-to-power ratio (thermal efficiency) of the power-producing technology. A typical solution for power generation driven by low-temperature heat is a bottoming power cycle. The Organic Rankine Cycle (ORC) is identified in the literature [8,9] as a robust technology for low-temperature heat recovery because of its flexible design, low maintenance cost, and nearly unsupervised operation. The ORC is a mature technology with maximum nominal electric capacities reaching

* Corresponding author.
E-mail address: tskiado@aua.gr (A. Skiadopoulos).

https://doi.org/10.1016/j.ecmx.2023.100432
Received 24 June 2023; Received in revised form 31 July 2023; Accepted 1 August 2023
Available online 6 August 2023

Nomenclature

p	Pressure [bar]
T	Temperature [°C]
A	Collectors' area [m^2]
h	Specific enthalpy [kJ/kg]
s	Specific entropy [kJ/kg-K]
G	Irradiance [W/m^2]
c_p	Specific heat [kJ/kg-K]
$\dot{m}$	Mass flow rate [kg/s]
$\dot{w}$	Power [kW]
x	Vapor quality [-]
E	Electricity [kWh]
e	Electricity price [€/kWh]
$\dot{Q}$	Heat transfer rate [kW]
C	Cost [€]
r	Discount rate [%]
L	Latitude [°]
P	Nominal power [kW]
sc	Specific cost [€/m^2] [€/kW]
hr	Hour angle [°]
R	Radiation tilt factor [-]
N	Lifetime [years]

Subscripts

in	Inlet
out	Outlet
is	Isentropic
ex	Expander
ev	Evaporator
con	Condenser
sub	Subcooling
pr	Preheating
pu	Pump
sat	Saturated
th	Thermal
ref	Reference
l	Liquid
amb	Ambient
m	Mean
col	Collector
d	Diffuse
b	Beam
tot	Total
inv	Investment
h	Horizontal
II	Second Law
av	Average
grid	Power grid

Greek letters

δ	Solar declination [°]
η	Efficiency [-]
β	Inclination angle [°]
α	Losses Coefficient [-]
μ	Specific emissions factor [kg/kWh]

Abbreviations

TFC	Trilateral Flash Cycle
FPC	Flat Plate Collector
ETC	Evacuated Tube Collector
HTF	Heat Transfer Fluid
CF	Cooling Fluid
WF	Working Fluid
PP	Pinch Point temperature difference [°C]
ORC	Organic Rankine Cycle
LCOE	Levelized Cost of Electricity
PBP	PayBack Period
GHG	GreenHouse Gas
PES	Primary Energy Savings
PEF	Primary Energy Factor

2 MW_{el} [10]. Several works have been published in the literature assessing the efficiency of the ORC, both numerically and experimentally, (indicatively see Refs. [11–17]) with different heat sources. The ORC operates on the same principle as the conventional water-steam Rankine cycle. However, its design is flexible since the Working Fluid (WF) of the cycle may be selected among a variety of substances. Thus, its thermal efficiency can be maximized based on the characteristics of the heat source and the operating pressure ratios. The drawback of the ORC is its rather low thermal efficiency, particularly as the temperature of the heat source drops. Several works have been published in the literature (e.g. [18–21]) to identify the reasons for the low thermal efficiency of the ORC and the means to increase it. The consensus is that in the ORC the exergy of the heat source is not fully exploited. The main exergy losses of the heat source are attributed to the isothermal WF evaporation at the evaporator of the power cycle. During this process, the temperature of the WF remains constant while the temperature of the Heat Transfer Fluid (HTF) drops. This leads to a sub-optimal match between the temperatures of the HTF and the WF at the evaporator. As a result, the operating pressure ratios of the WF and the generated power are diminished.

Different variations of the ORC have been studied in the literature to maximize the efficiency of the heat source's exergy utilization. Thermodynamic analysis indicates that the exergy of the heat source is optimally exploited when the power cycle obtains a trilateral shape [20,21]. In a trilateral cycle, the evaporation of the WF is omitted [20,21], and the temperature drop of the heat source leads always to a temperature rise of the WF. A promising trilateral power cycle is the TFC, initially conceptualized by Smith et al. [22] to exploit heat from geothermal fluids. The TFC consists of the same components as the ORC but the WF enters the expansion machine in the saturated liquid state, or partially evaporated in the generalized version of the TFC (also referred to as Partially Evaporating ORC in the relevant literature). There it undergoes two-phase expansion, also known as flashing, and generates power. In the TFC, the temperature profile of the WF at the evaporator can be matched to that of the HTF by increasing its mass flowrate. As a result, higher heat transfer rates are achieved at the evaporator because both fluids remain in the liquid state. The additional heat transferred to the WF increases the power output, and the exploitation of the heat source's exergy is enhanced. Many theoretical works assessing the performance of the TFC and comparing it to the ORC have been published in the literature. Smith et al. [22] concluded that the TFC can achieve a higher power output, that can reach up to 80%, than the ORC for different WFs in the temperature range of 100–200 °C of the HTF. This increase was observed when the expander's adiabatic efficiency reached values up to 75%. Fischer [19] showed that with the TFC a higher exergy efficiency of up to 29% can be obtained compared to the ORC for temperatures of the heat source up to 350 °C. Lecompte et al. [23] studied the performance of the generalized TFC and indicated that it can substantially improve the net power output, especially in cases where the isentropic efficiency of the pump is low. Iqbal et al. [24] showed that the TFC has at least 50% higher potential for power generation than the ORC, particularly when the HTF temperature is below 80 °C. Daniarta

et al. [25] compared the efficiency of the generalized TFC and the ORC for dry, wet, and isentropic (based on the slope of the vapor saturation curve) WFs and combinations of heat source and sink temperatures. They concluded that the generalized TFC can substantially improve the power output for given operating conditions.

Despite the acknowledged potential of the TFC, it is not yet technologically mature because there is a lack of fundamental knowledge on flashing. Flashing is complex to model and monitor because the liquid and vapor phases are in thermodynamic non-equilibrium throughout the process. Moreover, the presence of high amounts of liquid in the expander is challenging for state-of-the-art expanders because of the erosion risk. Therefore, in the literature, the two-phase expander is usually modeled as a black box with adiabatic efficiencies in the range achieved in the dry vapor region. Until now, only a few experimental works have been published focusing on two-phase expansion itself ([26–29]). All experimental works point out that higher vapor qualities at the expander's suction port lead to increased isentropic efficiencies. From a technological aspect, the conclusion from the literature review is that twin-screw expanders are the most promising solution for two-phase expansion. Indeed, these expanders can handle high mass flow-rates with reduced friction losses compared to turbines [30]. Moreover, they operate at lower rotational speeds than turbines, reducing, thus, the risk of erosion by the liquid WF [29].

In two-phase expansion modeling, only a few works have been published so far. Bianchi et al. [30] developed a 1-D numerical model simulating two-phase expansion in twin-screw expanders. In this work, the two phases are treated as a single fluid and they are assumed to be in thermodynamic equilibrium during flashing. The same approach is followed by Vasuthevan et al. [31] and Taniguchi et al. [32], also for the modeling of flashing in twin-screw expanders. Skiadopoulos et al. [33] developed a semi-empirical thermodynamic low-order model to simulate two-phase expansion in twin-screw expanders. In this work, non-equilibrium effects during flashing on the efficiency of the expander are considered. This is accomplished by applying a two-fluid modeling approach for the two phases and calculating the mass of generated vapor at their interface throughout flashing in the expander. The mass of generated vapor is calculated based on the thermal non-equilibrium between the two phases at the examined operational phase of the expander.

The present study assesses numerically the potential of the TFC for efficient solar energy conversion in Europe, by simulating the operation of small-scale Solar-TFC thermal power plants in different locations in the continent. Compared to the existing literature, the present work

- is the first to study solar thermal power plants with different types of collectors and the TFC as the bottoming power cycle
- applies a dedicated two-phase expansion model [33] to monitor the performance of the two-phase expander of the TFC under varying operating conditions
- focuses on the application of the Solar-TFC technology in different locations in Europe to provide location-specific techno-economic and environmental impact data

An integrated numerical tool is developed in the environment of Matlab (R2022b) to simulate the operation of the Solar-TFC unit in four cities in Europe, i.e. Athens, Copenhagen, Vienna, and Warsaw, with an hourly timestep. The efficiency equations of the solar collectors, a thermodynamic model of the TFC power cycle, and the two-phase expansion model [33] are coupled in the developed numerical model. Initially, the effect of two-phase expansion efficiency on the performance of the TFC and the Solar-TFC unit is presented. Thereafter, the operation of the Solar-TFC is optimized at each timestep to maximize the total solar energy conversion efficiency. Meteorological data for the selected locations are taken from the PVGIS database [34], whereas solar heat is assumed to be provided by ETCs and FPCs. Following the optimization of the Solar-TFC unit's operation, its economics and environmental impact are studied as a function of the location, collector type and area, and annual electricity output.

The remainder of the paper is organized as follows. In Section 2 the architecture of the modeled Solar-TFC unit is presented, along with the inputs for the simulations and the utilized performance evaluation indexes. The modeling methodology is presented in Section 3. In Section 4, the simulations' results are presented and discussed in detail. In the Section 5, the main outcomes and conclusions of this work are given.

2. Problem description

A schematic layout of the modeled Solar-TFC unit is presented in Fig. 1. Solar heat is transferred from the collectors to the evaporator of the TFC through the HTF. The thermodynamic states of the WF in the TFC (numbered 1 ÷ 4) are presented in Fig. 1. In the evaporator of the TFC, the WF is heated up (2 → 3), and thereafter it flows, in the saturated liquid state or as a two-phase mixture, to the two-phase expander. At the expander, flashing occurs (3 → 4), and power is generated. The two-phase mixture at the expander's discharge dissipates heat to the Cooling Fluid (CF) as it flows through the condenser (4 → 1). Finally, the WF is pumped to the operating pressure of the evaporator (1 → 2), and the power cycle starts anew.

At each timestep, the boundary conditions are the total solar irradiance G_{tot} on the collectors' surface, and the ambient temperature T_{amb}. The identified operational degrees of freedom of the Solar-TFC unit (details in Section 3) are listed in Table 1, along with their descriptions and allowed ranges in this work. Based on the value of T_m, H_20 pressurized at 3 bar, to avoid partial evaporation in the solar loop, is selected as the HTF. R245fa is selected as the WF of the TFC because it has demonstrated very good thermodynamic behavior within the range of temperature and operating pressure ratios of low-temperature Solar-ORC power units [15,17]. Finally, Air is selected as the CF to study the influence of ambient conditions on the Solar-TFC unit.

The utilized evaluation indexes of the Solar-TFC unit are listed in Table 2. Four different cities in Europe (Athens, Copenhagen, Vienna, and Warsaw), and two different types of solar collectors are examined (ETCs and FPCs) for an in-depth techno-economic and environmental impact analysis.

3. Methodology

3.1. Solar-TFC modeling

3.1.1. Solar collectors

Solar heat is provided to the TFC by ETC and FPC collectors to study the effect of the collector type on the total solar energy conversion efficiency, economics, and environmental impact of the power plant. The Thermomax DF 100-30, developed by Kingspan Thermomax [35], and the Vitosol 300-F, developed by Viessmann [36], are selected as the ETCs and FPCs, respectively. The modeling parameters of the selected ETC [37] and FPC [38] collectors are listed in Table 3, where A_{col} denotes the total area of the collectors.

The inclination angle β of the collectors is selected to maximize the annually absorbed solar irradiance at the selected locations, based on the PVGIS database [34]. The values of β for the four examined cities are listed in Table 4.

The thermal efficiency η_{col} of the collectors is calculated by Eq. (1), where T_{amb} is the ambient temperature.

$$\eta_{col} = \eta_o - a_1 \bullet \frac{(T_m - T_{amb})}{G_{tot}} - a_2 \bullet \frac{(T_m - T_{amb})^2}{G_{tot}} \quad (1)$$

η_{col} is also given by given by Eq. (2), where $\dot{Q}_{ev}$ is the heat gain of the collectors from the solar irradiance. Assuming steady-state operation of the Solar-TFC unit, and neglecting heat losses through the loop, $\dot{Q}_{ev}$ is equal to the heat transfer rate from the solar field to the evaporator of

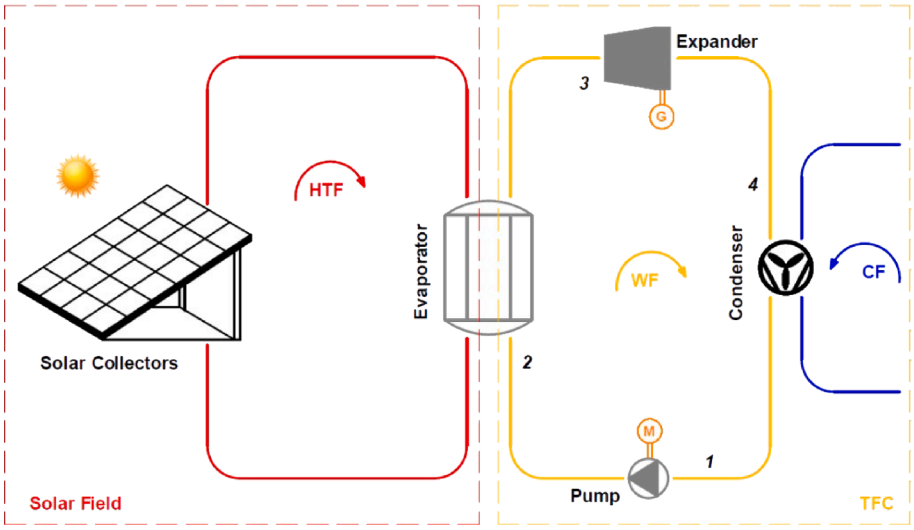

Fig. 1. Schematic layout of the Solar-TFC system.

Table 1
Parameters for Solar-TFC simulations.

Parameter	Symbol [Units]	Range
Average collectors' temperature	T_m[°C]	80–120
Quality of the WF at the suction port of the expander	x_3[-]	0–1

Table 2
Solar-TFC unit evaluation indexes.

Index	Symbol [Units]
Expander isentropic efficiency	$\eta_{ex,is}$[-]
Thermal efficiency of the TFC	η_{th}[-]
Total solar energy conversion efficiency	η_{tot}[-]
Second-law efficiency	η_{II}[-]
Levelized cost of electricity	$LCOE$[€/kWh]
Payback period	PBP[years]
Primary energy savings	PES[kWh]
Greenhouse gas emissions reduction	ΔGHG[%]

Table 3
Modeling parameters of the Solar collectors.

Coefficient	Symbol [Units]	Value	
		ETC	FPC
Optical efficiency at normal incidence	η_o[-]	0.779	0.803
First-order thermal losses	a_1[W/m^2-K]	1.070	3.770
Second-order thermal losses	a_2[W/m^2-K^2]	0.0135	0.0156
Collectors' area – specific HTF mass flowrate	$\dot{m}_{htf}/A_{col}$	0.030	0.030

Table 4
Inclination angle β of the Solar collectors.

City	Athens	Copenhagen	Vienna	Warsaw
β[°] (ETC&FPC)	33	44	41	41

the TFC.

$$\eta_{col} = \frac{\dot{Q}_{ev}}{A_{col} \bullet G_{tot}} \tag{2}$$

T_m is assumed to be equal to the average temperature of the HTF flowing in the solar loop. This assumption is expressed by Eq. (3), where $T_{htf,in}$ and $T_{htf,out}$ represent the temperature of the HTF flowing in and out of the solar cooling loop, respectively.

$$T_m = \frac{T_{htf,in} + T_{htf,out}}{2} \tag{3}$$

$\dot{Q}_{ev}$ is given by Eq. (4), where $c_{p,htf}$ is the specific heat capacity, under constant pressure, of the HTF, and $\dot{m}_{htf}$ is its flowrate.

$$\dot{Q}_{ev} = \dot{m}_{htf} \bullet c_{p,htf} \left(T_{htf,out} - T_{htf,in}\right) \tag{4}$$

The total irradiance G_{tot} on the inclined surface of the collectors is given by Eq. (5). In Eq. (5), G_b and G_d stand for the beam irradiance normal on the collectors, and the diffuse irradiance, respectively. Ground-reflected irradiance was not considered in the numerical modeling.

$$G_{tot} = G_b + G_d \tag{5}$$

G_b is extracted from the available meteorological data at the examined locations, and it is calculated by Eq. (6), where G_h is the beam irradiance on a horizontal surface, and R_b is the beam radiation tilt factor.

$$G_b = G_h \bullet R_b \tag{6}$$

R_b is given at each time instance by applying Eq. (7). In Eq. (7), L is the local latitude, δ the solar declination, and hr is the hour angle. Details about the calculation of the solar angles are presented in the work of Kalogirou [39].

$$R_b = \frac{\sin(L-\beta) \bullet \sin(\delta) + \cos(L-\beta) \bullet \cos(\delta) \bullet \cos(hr)}{\sin(L) \bullet \sin(\delta) + \cos \bullet (L) \bullet \cos(\delta) \bullet \cos(hr)} \tag{7}$$

3.1.2. TFC power cycle

A qualitative Temperature- Entropy (T-s) diagram of the TFC power cycle with R245fa as the WF is presented in Fig. 2. In this diagram, the thermodynamic processes of the WF in the TFC are drawn. These are:

1) 1 → 2: Pumping
2) 2 → 3: Heat absorption at constant pressure p_{ev}
3) 3 → 4: Expansion
4) 4 → 1: Heat rejection at constant pressure p_{con}

The WF is sub-cooled by ΔT_{sub} at the suction port of the pump to prevent cavitation. Heat is transferred to the evaporator of the TFC engine by the HTF of the solar loop, leading to a drop in its temperature from $T_{htf,out}$ to $T_{htf,in}$. An air-cooled condenser is assumed to dissipate

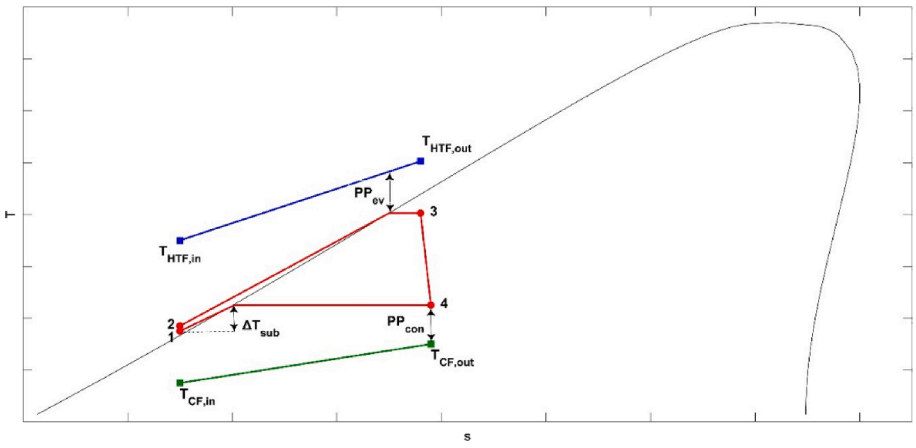

Fig. 2. Qualitative T-s diagram of the TFC with R245fa as the WF.

heat to the ambient, resulting in the temperature rise of the (CF) from $T_{cf,in}$ to $T_{cf,out}$. In the present work, the term TFC refers to power cycles in which the quality of the WF at the onset of expansion is between 0 and 1.

In Table 5, the selected modeling parameters for the TFC, along with their values and descriptions, are listed. Typical values for PP_{ev}, PP_{con}, and $\eta_{pu,is}$ in power cycle modeling are assumed [9].

Assuming negligible heat losses at the TFC evaporator, $\dot{Q}_{ev}$ will be equal to the heat absorbed by the WF of the TFC, as in Eq. (8)

$$\dot{Q}_{ev} = \dot{m}_{wf} \bullet (h_3 - h_2) \tag{8}$$

where $\dot{m}_{wf}$ is the mass flowrate of the WF, whereas h_3 and h_2 are the specific enthalpies of the WF at thermodynamic states 2 and 3 of the power cycle, respectively.

The temperature T_4 of the WF at the onset of condensation is derived from

PP_{con}, as in Eq. (9)

$$T_4 = T_{cf,out} + PP_{con} \tag{9}$$

where $T_{cf,out}$ is the temperature of the CF at the outlet of the condenser's cooling loop, given by Eq. (10). In Eq. (10), $T_{cf,in}$ is the temperature of the CF at the inlet of the cooling loop, equal to T_{amb}, for the case of the air-cooled condenser.

$$T_{cf,out} = T_{cf,in} + \Delta T_{CF} \tag{10}$$

After applying Eq. (9), p_{con} is readily calculated, as the saturation pressure of the WF at T_4. The coupling between the TFC and the solar loop is accomplished by

PP_{ev}, as expressed by Eq. (11). In Eq. (11) $T_{htf,pr}$ is the temperature of the HTF at the end of the preheating stage, and $T_{sat,wf}(p_{ev})$ is the saturation temperature of the WF at p_{ev}.

$$T_{htf,pr} = T_{sat,wf}(p_{ev}) + PP_{ev} \tag{11}$$

Additionally to the energy balance expressed by Eq. (8), Eq. (12) must be satisfied, wherein $\dot{Q}_{pr}$ is the heat transfer rate from the HTF to the WF during the preheating stage, and $h_{l,sat}(p_{ev})$ is the enthalpy of the saturated liquid at p_{ev}.

$$\dot{Q}_{pr} = \dot{m}_{wf} \bullet \left(h_{l,sat}(p_{ev}) - h_2\right) = \dot{m}_{htf} \bullet c_{p,htf} \bullet \left(T_{htf,pr} - T_{htf,in}\right) \tag{12}$$

The numerical procedure for the determination of $\dot{m}_{wf}$ and p_{ev}, for a desired quality x_3 of the two-phase mixture at the onset of expansion is as follows. The value of p_{ev} is varied iteratively in a stepwise manner. For a guess intermediate value of p_{ev}, the saturation temperature $T_{sat,wf}(p_{ev})$ of the WF is calculated, and subsequently, $T_{htf,pr}$ is derived by applying Eq. (11). Thereafter, two values for $\dot{m}_{wf}$ are calculated by simultaneously applying Eqs. (8) and (12). The iterations on p_{ev} terminate when the two values converge.

After the values of $\dot{m}_{wf}$ and p_{ev} have been determined, the thermodynamic low-order two-phase expansion model developed by Skiadopoulos et al. [33] is run. The outcome of the two-phase expansion simulation is the rotational speed of the expander that maximizes efficiency for the given mass flowrate, quality at the suction port of the expander and operating pressure ratio, and the specific enthalpy h_4 of the WF at the discharge port. Thereafter, the isentropic efficiency $\eta_{ex,is}$ of expansion is calculated by Eq. (13). In Eq. (13), $h_{4,is}$ is the specific enthalpy of the WF corresponding to its isentropic two-phase expansion from state 3 to p_{con}.

$$\eta_{ex,is} = \frac{h_3 - h_4}{h_3 - h_{4,is}} \tag{13}$$

The power $\dot{w}_{ex}$ generated by the two-phase expander is given by Eq. (14)

$$\dot{w}_{ex} = \dot{m}_{wf} \bullet (h_3 - h_4) \tag{14}$$

whereas the power $\dot{w}_{pu}$ absorbed by the pump is calculated by applying Eq. (15), in which h_1 is the specific enthalpy of the WF at its suction.

$$\dot{w}_{pu} = \dot{m}_{wf} \bullet (h_2 - h_1) \tag{15}$$

h_2 is derived by applying the formula for the isentropic efficiency $\eta_{pu,is}$ of the pump, as in Eq. (16).

$$\eta_{pu,is} = \frac{h_{2,is} - h_1}{h_2 - h_1} \tag{16}$$

In Eq. (16), $h_{2,is}$ is the specific enthalpy of the WF corresponding to its isentropic pumping from p_{con} to p_{ev}. The thermal efficiency η_{th} of the TFC is given by Eq. (17), in which $\dot{w}_{net}$ is the net power generated by the TFC.

$$\eta_{th} = \frac{\dot{w}_{net}}{\dot{Q}_{ev}} = \frac{\dot{w}_{ex} - \dot{w}_{pu}}{\dot{Q}_{ev}} \tag{17}$$

Table 5
Modeling parameters of the TFC cycle.

Parameter	Symbol [Units]	Value
Pinch point temperature difference at the evaporator	PP_{ev}[°C]	5
Pinch point temperature difference at the condenser	PP_{con}[°C]	5
Pump isentropic efficiency	$\eta_{pu,is}$[-]	0.75
Heat Transfer Fluid	HTF [-]	H_2O
Working Fluid	WF [-]	R245fa
Cooling Fluid	CF [-]	Air
Temperature rise of the Cooling Fluid	ΔT_{CF}[°C]	10
WF sub-cooling at pump suction	ΔT_{sub}[°C]	5

The heat transfer rate $\dot{Q}_{con}$ at the condenser is calculated by Eq. (18), leading to the reckoning of the necessary mass flowrate $\dot{m}_{cf}$ of the CF. In Eq. (18) $c_{p,cf}$ is the specific heat capacity, under constant pressure, of the CF.

$$\dot{Q}_{con} = \dot{m}_{wf} \bullet (h_4 - h_1) = \dot{m}_{cf} \bullet c_{p,cf} \bullet \Delta T_{CF} \tag{18}$$

3.1.3. Performance indicators

The total solar energy conversion efficiency η_{tot} of the Solar-TFC unit is given by Eq. (19).

$$\eta_{tot} = \eta_{col} \bullet \eta_{th} = \frac{\dot{w}_{net}}{A_{col} \bullet G_{tot}} \tag{19}$$

On the other hand, its exergy efficiency η_{II} is given by Eq. (20), where $T_{ref,sun}$ represents the reference temperature of the sun. In this work, $T_{ref,sun}$ is taken equal to 5770 K [17]. The denominator in Eq. (20) represents the exergy input from the sun to the Solar-TFC system. It must be noted that, as in all solar thermal power units, the extremely high value of $T_{ref,sun}$, compared to T_{amb}, leads to very low values of η_{II}.

$$\eta_{II} = \frac{\dot{w}_{net}}{\left(1 - \frac{T_{amb}}{T_{ref,sun}}\right) A_{col} \bullet G_{tot}} \tag{20}$$

By integrating Eqs. (17), (19), and (20) over a period, the average thermal efficiency $\eta_{th,av}$, total efficiency $\eta_{tot,av}$, and exergy efficiency $\eta_{II,av}$ for the respective period is obtained.

3.1.4. Solar-TFC optimization

The governing equations presented in the previous Sections are formulated in an integrated numerical tool in the environment of Matlab (R2022b). The simulation and optimization toolkits of Matlab are utilized to build the software. The two-phase expansion model [33] is incorporated in the TFC model (details about the coupling procedure in Section 3.1.2) as an external function. The thermodynamic properties of the HTF, the WF, and the CF are calculated in Matlab by the Coolprop [40] open-source library wrapper.

By analyzing the set of Solar-TFC governing equations, two operational degrees of freedom are identified, i.e. T_m and x_3. An hourly timestep is selected for the simulations. The operation of the Solar-TFC unit is optimized at each timestep by applying the genetic algorithm of the Matlab optimization toolkit (details can be found in Matlab documentation). A simplified schematic flowchart of the optimization algorithm of the Solar-TFC applied in this study is presented in Fig. 3. At each hour throughout the year the inputs for the simulation are the HTF, the WF, the CF, the geographical and collectors' data, and T_{amb}. By combining the geographical and collectors' data (type and inclination angle β), the value of G_{tot} can be readily calculated. The Solar-TFC unit is allowed to operate when G_{tot} exceeds 400 W/m^2. For the given inputs the optimization process is as follows. Guess values are assigned to T_m and x_3 by the genetic algorithm, and the Solar-TFC equations, coupled with the two-phase expansion model, are solved iteratively. The objective of the optimization algorithm is to maximize η_{tot} (objective function) at each timestep.

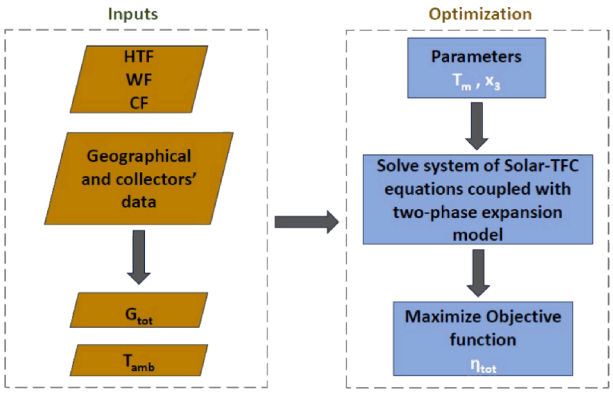

Fig. 3. Schematic flowchart of the Solar-TFC operation optimization algorithm.

3.2. Economics

In this work, the economics of the Solar-TFC unit is studied as a function of A_{col}. Two widely used indexes in the techno-economic analysis of energy systems, i.e. the *LCOE* and the PayBack Period (*PBP*), are applied.

LCOE is given by Eq. (21). In Eq. (21), C_{inv} is the total initial investment cost, N is the anticipated lifetime of the Solar-TFC system, E_{tot} is the total electricity produced at year i, M the annual maintenance cost at year i, and r the annual discount rate. In this work, it is assumed that E_{tot}, as well as M and r remain constant throughout N. C_{inv} is given by Eq. (22), where sc_{tfc} and sc_{col} are the specific costs of the TFC and the collectors, respectively, whereas P_{tfc} is the nominal electric capacity of the TFC.

$$LCOE = \frac{C_{inv} + \sum_{i=1}^{N} \frac{M}{(1+i)^r}}{\sum_{i=1}^{N} E_{tot}} \tag{21}$$

$$C_{inv} = sc_{tfc} \bullet P_{tfc} + sc_{col} \bullet A_{col} \tag{22}$$

PBP is the quotient of C_{inv} to the net annual average income, assuming that the generated electricity is sold to the grid, and it is expressed by Eq. (23). In Eq. (23), e_{grid} denotes the price of electricity.

$$PBP = \frac{C_{inv}}{E_{tot} \bullet e_{grid} - M} \tag{23}$$

The values of the economics analysis parameters, along with their symbols and units, are listed in Table 6. Moreover, the value of sc_{col} for the selected ETCs [16] and FPCs [41] are listed in Table 7.

Concerning the value of sc_{tfc}, it is assumed that it is a function of P_{tfc}. The first step for the calculation of sc_{tfc} is the determination of the Solar-TFC unit's design specifications, listed in Table 8. At the design point, the value of η_{col} is calculated for the ETCs and FPCs by applying Eq. (1). Thereafter, by varying A_{col}, the value of $\dot{Q}_{ev}$ is calculated by Eq. (2), and, based on the design value of η_{th}, P_{tfc} is estimated. Finally, the methodology of Braimakis et al. [42] is applied to calculate sc_{tfc}, for the estimated values of P_{tfc}. The calculated values of sc_{tfc} and P_{tfc} as a function of A_{col} for the ETCs and FPCs are listed in Table 9.

3.3. Environmental impact analysis

The environmental impact of the Solar-TFC system is assessed by evaluating the Primary Energy Savings (*PES*), and the reduction ΔGHG in GreenHouse Gas (GHG) emissions on an annual basis. *PES* are calculated by applying Eq. (24).

$$PES = PEF \bullet E_{tot} \tag{24}$$

In Eq. (24), *PEF* represents the primary energy factor, which expresses the primary energy utilized in central power stations to produce 1 kWh of electricity for the end user. *PEF* is country-specific, and it is a function of the efficiency of central power stations and energy transmission networks. The annual reduction ΔGHG in GHG is given by Eq.

Table 6
Parameters of the economic analysis.

Parameter	Symbol [Units]	Value
Lifetime	N[yr]	20
Annual discount rate	r[%]	5
Annual maintenance cost	M[€]	$0.01C_{inv}$
Electricity price	e_{grid}[€/kWh]	0.30

Table 7
Specific cost sc_{col} for the ETCs and FPCs.

Collector	ETC	FPC
sc_{col} [€/m^2]	260	210

Table 8
Design specifications for the Solar-TFC system.

Collector	ETC	FPC
T_m [°C]	110	90
T_{amb} [°C]	20	20
G_{tot} [W/m^2]	1000	1000
η_{th} [-]	0.10	0.10

Table 9
P_{tfc} and sc_{tfc} as a function of A_{col} for ETCs and FPCs.

A_{col} [m^2]	P_{tfc} [kW]		sc_{tfc} [€/kW]	
	ETC	FPC	ETC	FPC
200	11.50	11.10	4850	4880
300	17.20	16.70	4270	4310
400	22.90	22.30	3770	3820
500	28.70	27.80	3330	3390

(25), in which μ_{CO_2} is the GHG emission intensity of electricity production.

$$\Delta GHG = \mu_{CO_2} \bullet E_{tot} \tag{25}$$

The values of *PEF* [43] and μ_{CO_2} [44] for the examined locations are listed in Table 10, and they are considered constant throughout the entire operational lifetime N of the Solar-TFC unit.

4. Results & discussion

4.1. Effect of two-phase expansion on TFC and Solar-TFC

Before presenting the results from the optimization of the Solar-TFC unit's operation, a short section is dedicated to describing the effect of two-phase expansion on the efficiency of the TFC, and, subsequently, the Solar-TFC. To this end, parametric Solar-TFC simulations were performed, with T_m and x_3 as the parameters. Specifically, the Solar-TFC numerical tool was run without the optimization feature. Instead, the set of Solar-TFC governing equations was solved for different combinations of T_m and x_3, and the TFC evaluation indexes were documented for all resulting operating points, and not only the optimal. For the indicative simulations performed for this section, it has been assumed that $G_{tot} = 1000 W/m^2$, $A_{col} = 200 m^2$, and $T_{amb} = 20^o C$, while ETCs was the solar heat source.

The main component of interest in the TFC is the two-phase expander. This is because the performance of all the other components, i.e. pump and heat exchangers, has been studied in depth in the ORC literature. Thus, the focus is on the efficiency of the two-phase expander. The variation of $\eta_{ex,is}$ as a function of x_3, for different values of T_m is presented in Fig 4a. For all values of T_m, $\eta_{ex,is}$ obtains its minimum as x_3 approaches zero. This happens for two reasons. First, the reduction of x_3 leads in increased $\dot{m}_{wf}$ values in the TFC. The elevated $\dot{m}_{wf}$ does not necessarily flow through the expansion chamber of the modeled expander because of the limitation posed by its swept volume value (details about the geometrical data of the modeled twin-screw expander are available in the work of Skiadopoulos et al. [33]). Therefore, as $\dot{m}_{wf}$ increases, a significant fraction of it will flow through the expander's available leakage paths. Second, as the amount of liquid at the onset of expansion increases, the pressure losses at the expander's suction port are higher because of the reduced WF's specific volume [27,33]. As a result, the WF pressure ratio at the expansion chamber is lowered, with a negative effect on $\dot{w}_{net}$ and $\eta_{ex,is}$.

For a given value of x_3, $\eta_{ex,is}$ is strongly dependent on T_m because it contributes indirectly to the reckoning of p_{ev} (details in Section 3.1.2). For a known value of p_{ev}, the operating pressure ratio of the TFC is readily determined because p_{con} is a function of T_{amb} (see Eq. (9)). The combination of the operating pressure ratio with $\dot{m}_{wf}$ determines the volume ratio of the WF in the expansion chamber. When the WF volume ratio approaches the expander's built-in volume ratio, $\eta_{ex,is}$ is maximized, and this is accomplished for a specific value of T_m. Increasing T_m does not necessarily have a positive effect on $\eta_{ex,is}$, because of over-expansion, whereas reduced values of T_m may lead to under-expansion [33]. Hence, there is an optimal combination of T_m and x_3, for a known value of T_{amb}, that leads to the maximization of $\eta_{ex,is}$.

In Fig 4b the variation of η_{II} as a function of x_3 is plotted to highlight the effect of two-phase expansion on the efficiency of the Solar-TFC unit. A similar trend with the variation of $\eta_{ex,is}$ is observed. Indeed, for all values of T_m, η_{II} is maximized when $\eta_{ex,is}$ is optimal. This is because as $\eta_{ex,is}$ increases, the power output of the TFC increases. However, η_{II} becomes maximum at a T_m value of 110 °C, which is higher than the one (100 °C) for which $\eta_{ex,is}$ obtains its global maximum for this set of simulations. This occurs because at T_m equal to 110 °C η_{col} is higher for the examined ambient conditions. As a result, a higher $\dot{Q}_{ev}$ is transferred to the TFC, and the value of η_{II} is increased.

Table 10
PEF and electricity production GHG emission intensity.

Parameter	Symbol [Units]	Value			
		Greece	Denmark	Austria	Poland
Primary Energy Factor	*PEF*[-]	2.353	1.228	1.548	2.114
Electricity production related GHG emission intensity	μ_{CO_2} [kg CO_2-eq./kWh]	0.466	0.112	0.079	0.711

4.2. Solar-TFC

4.2.1. Performance optimization

Solar-TFC optimization simulations are performed with an hourly timestep for all the selected locations and both collector types, based on the algorithm presented in Section 3.1.4. The parameters T_m and x_3 vary within the range listed in Table 1. Initially, two test cases are simulated where the operation of the Solar-TFC is optimized. The purpose is to provide a visualization of the numerical model's output. In Table 11 the Solar-TFC parameters and the selected TFC variables for the resulting optimal operating points are listed. Please note that indexes correspond to the thermodynamic states of the WF, as drawn in Fig. 2. The selected ambient conditions that determine the test cases are also presented in Table 11. The results presented in Table 11 highlight the potential of the developed model to provide a clear and concise view of the Solar-TFC unit's dynamics and determine the optimal operating point.

In Fig. 5 and Fig. 6 the optimal T_m for the ETCs and FPCs, respectively, throughout the year, for all the examined cities, is plotted. The ETCs can operate at higher T_m for longer because their thermal losses toward the ambient are lower than the ones of the FPCs. On the other hand, the FPCs perform more efficiently when T_m tends to the lower allowable value of 80 °C. Higher optimal T_m values are more frequent in Athens because of the increased values of solar irradiance for more days in the year. However, increased T_m does not necessarily correspond to higher power output in the case of the modeled Solar-TFC unit because the operating pressure ratio of the TFC depends also on T_{amb}.

The optimal x_3 at the suction port of the expander throughout the

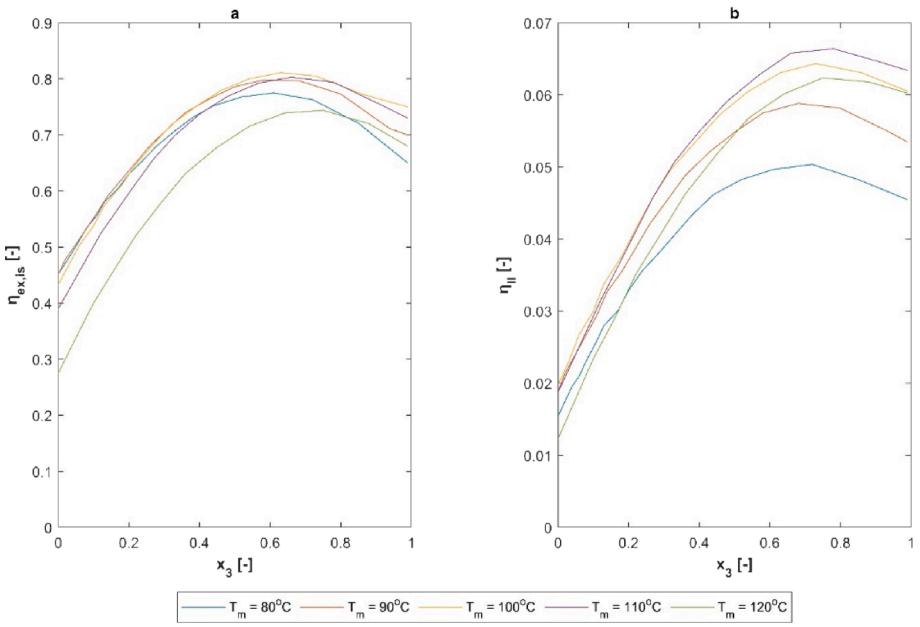

Fig. 4. a) $\eta_{ex,is}$ and b) η_{II} as a function of x_3 for different values of T_m, and ETCs as the solar field. $T_{amb} = 20^oC$, $G_{tot} = 1000W/m^2$, and $A_{col} = 200m^2$.

Table 11
Solar-TFC parameters and TFC variables for indicative optimal operating points.

Parameter/ TFC Variable [Units]	Case 1 $G_{tot} = 850W/m^2$, $T_{amb} = 12^oC$		Case 2 $G_{tot} = 1000W/m^2$, $T_{amb} = 35^oC$	
	ETCs	FPCs	ETCs	FPCs
T_m [°C]	100.87	87.53	119.78	114.95
x_3 [-]	0.77	0.73	0.74	0.72
p_{ev} [bar]	11.51	8.37	17.44	15.72
p_{con} [bar]	1.64	1.64	3.40	3.40
T_1 [°C]	22.73	22.73	44.57	44.57
T_2 [°C]	23.25	23.08	45.41	45.31
T_3 [°C]	95.83	82.36	115.00	110.02
T_4 [°C]	27.73	27.73	49.57	49.57
η_{th} [-]	0.110	0.095	0.097	0.091
η_{tot} [-]	0.060	0.045	0.056	0.044

year is plotted in Fig. 7 and Fig. 8, where the ETCs and the FPCs, respectively, provide solar heat to the TFC. The optimal values of x_3 lie in the region between 0.68 and 0.85, with slightly lower values observed when the FPCs are utilized. As explained in Section 4.1, higher quantities of vapor at the onset of expansion lead to increased $\eta_{ex,is}$, and, indirectly η_{th} and η_{tot}. Values higher than 0 for x_3 have a positive effect on $\eta_{ex,is}$. However, the optimal values will depend on the geometric characteristics of the specific expander. Lower values of x_3 than the ones presented in Fig. 7 and Fig. 8 will be optimal when expanders with higher built-in volume ratios and swept volumes than the twin-screw expander modeled in this work are used (Fig. 9).

4.2.2. Efficiency and annual electricity output

The variation of the monthly and annual average thermal efficiency $\eta_{th,av}$ of the TFC in all the examined locations, and for both types of modeled solar collectors, is presented in Fig. 10. A similar pattern is observed in all four cities for both ETCs and FPCs. Better performance of the TFC is observed during autumn and fall. This is because solar irradiance is high during these seasons, whereas T_{amb} is not as high as in summer. Therefore, the operating pressure ratio of the TFC is not necessarily optimal during summer, even though the solar irradiance is maximized. Quantitatively, approximately equal annual $\eta_{th,av}$ values are estimated for the ETCs and FPCs in all the examined locations, rising to 10% and 8%, respectively. The efficiency of the TFC is higher when heat is provided by the ETCs because, typically, they operate at higher T_m than the FPCs for given T_{amb}.

An analogous behavior to $\eta_{th,av}$ of the TFC is observed for the monthly and annual average total efficiency $\eta_{tot,av}$ of the Solar-TFC system, as presented in Fig. 10, with maximum values during months with high availability of solar energy and average values of T_{amb}. Approximately, the annual $\eta_{tot,av}$ reaches 5% in all examined cities when the ETCs act as the heat source and 3% when the FPCs are used.

In Fig. 11, the annual average values for $\eta_{II,av}$ of the Solar-TFC unit for all the examined locations, and both types of collectors are presented. Interestingly, similar values are estimated for the four cities, indicating that the exergy efficiency of the system is not significantly affected by the geographical coordinates. Moreover, the utilization of the ETCs results in systematically more efficient utilization of the heat source because of their better efficiency in solar heat harvesting. $\eta_{II,av}$ ranges among the four cities between 5 and 5.3% when the ETCs are utilized and between 3.2 and 3.6 % when the FPCs provide solar heat to the TFC.

In Fig. 12, the collectors' area- specific total annual electricity output E_{tot}/A_{col} for all the examined cities is presented, for both the ETCs and FPCs. The utilization of the ETCs results in increased annual electricity output because the values of η_{col} are substantially higher than the ones of the FPCs. When the ETCs provide heat to the Solar-TFC unit, the annual electricity output is estimated to be, based on the location, about 45–55% higher, with the FPCs performing more efficiently in Athens.

4.3. Economic assessment

The economics of the system is assessed as a function of A_{col}. Based on the design specifications of the Solar-TFC system in Table 8, the value of sc_{tfc} is obtained (see Table 9), resulting in the determination of C_{inv} for different values of A_{col}, for given values of sc_{col} (see Table 7). *LCOE* and *PBP* versus A_{col} for the four examined cities and the dirrerent types of solar collectors are presented in Fig. 13 and Fig. 14, respectively.

The economics of the Solar-TFC unit is improved as its scale increases because the investment cost for the TFC is lower as P_{tfc} increases. Optimal economic performance is observed in Athens for both the ETCs and FPCs, because of the increased annual electricity output for the same A_{col}, compared to the other examined cities. The utilization of the ETCs

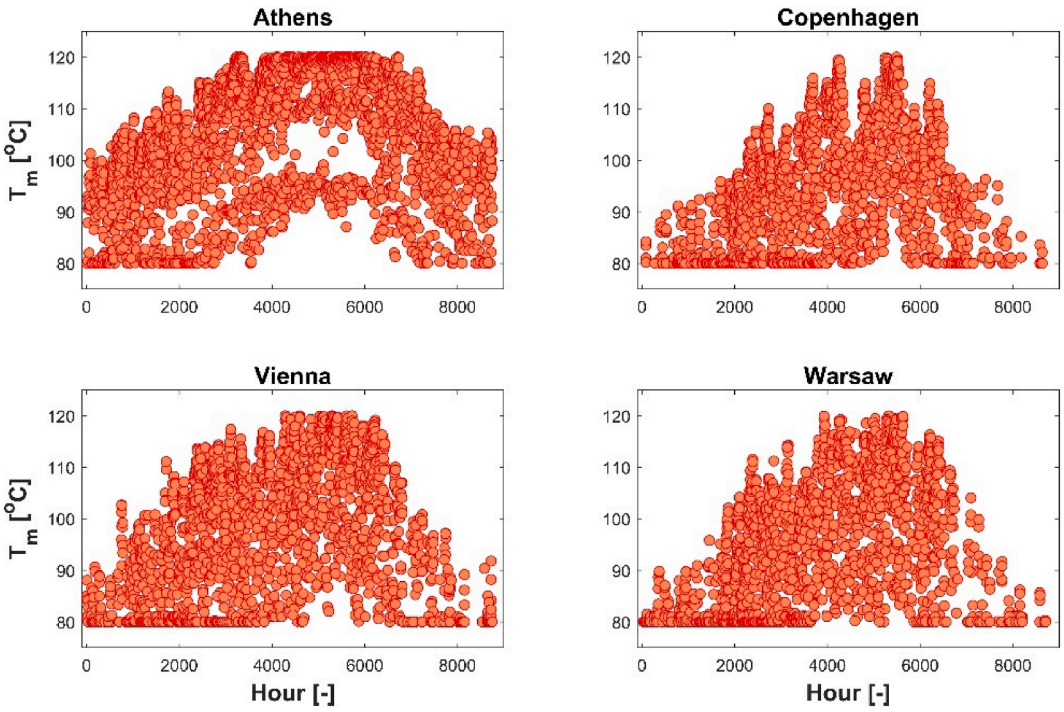

Fig. 5. Variation of optimal T_m of the ETCs throughout the year.

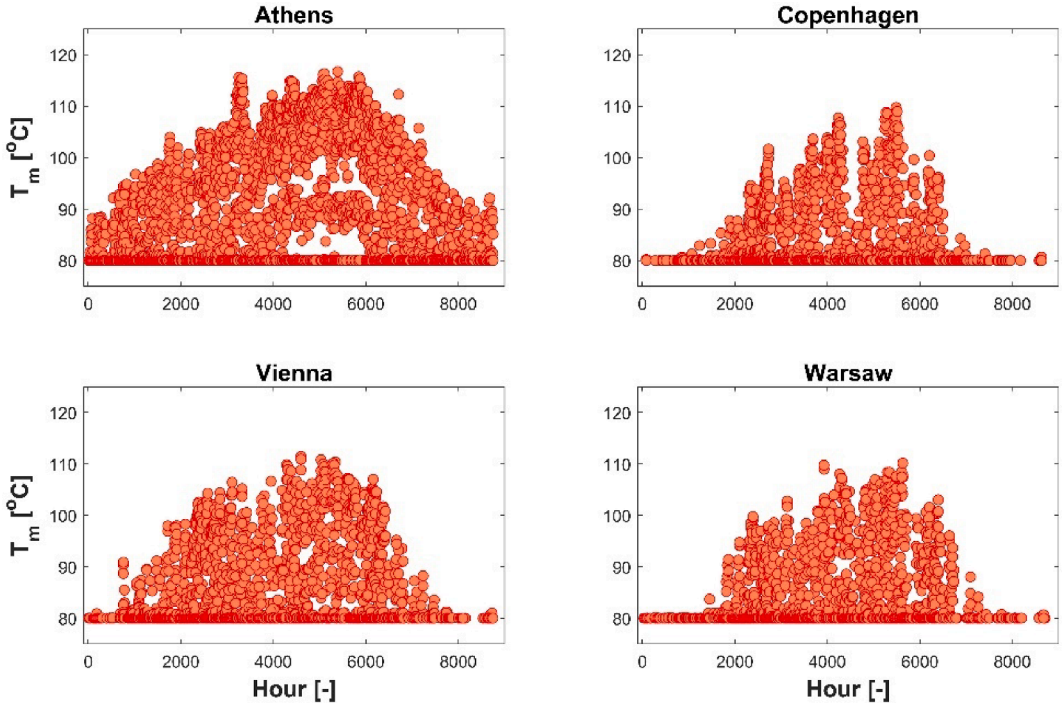

Fig. 6. Variation of optimal T_m of the FPCs throughout the year.

results in a better economic performance of the Solar-TFC system. This occurs because their higher initial investment cost is outweighed by the increased annual electricity output they induce.

The Solar-TFC unit can achieve competitive *LCOE* values to the ones of Solar-ORC systems, that range between 0.25 and 0.95 €/kWh [15–17]. With the assumptions made in this work, the *PBP* seems competitive only when ETCs are utilized, but a more strict analysis is necessary. Additional values that need to be considered for a more detailed calculation of *PBP* are the country-specific values of e_{grid}, and European policies to assist the penetration of renewable energy sources in the energy mix.

4.4. Environmental assessment

The variation of PES/A_{col} and $\Delta GHG/A_{col}$ for the four studied cities, and both types of solar collectors are presented in Fig. 15. In Athens, the environmental impact is maximized because of the combination of higher E_{tot}, low efficiency of central thermal power stations, and

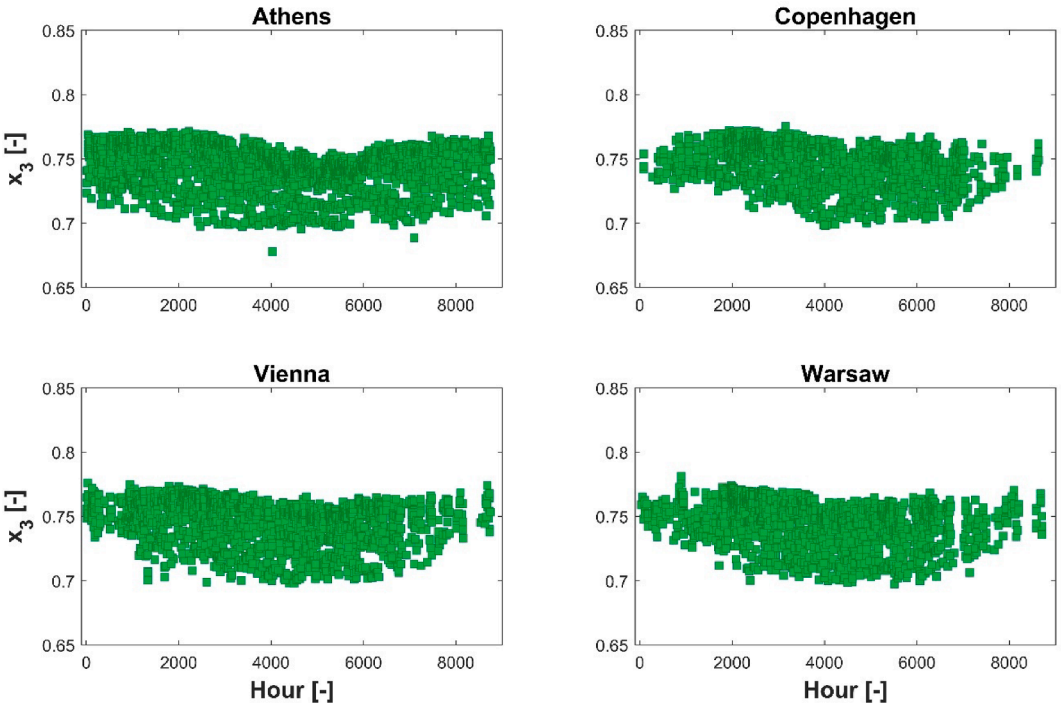

Fig. 7. Variation of optimal x_3 throughout the year. ETCs as the solar field.

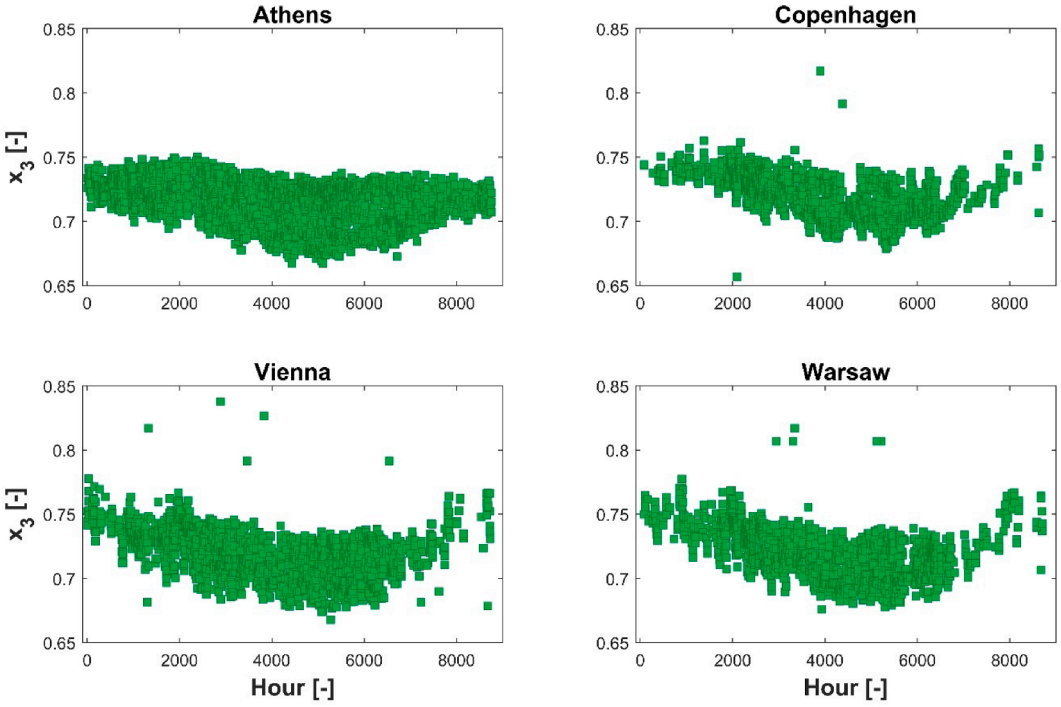

Fig. 8. Variation of optimal x_3 throughout the year. FPCs as the solar field.

increased GHG emissions related to electricity production in Greece. On the other hand, the environmental impact of the Solar-TFC unit would be much lower in Vienna and Copenhagen, considering the efficient performance of electric power systems in Austria and Denmark. In Warsaw, the wide-scale application of Solar-TFC systems would have a substantial environmental effect, particularly because of the extremely high electricity production-related GHG emissions in Poland.

5. Conclusions

The target of this study was to numerically investigate the potential of the TFC, a promising high-efficiency alternative to the ORC, for the efficient conversion of solar heat to power in Europe. An integrated numerical model was developed and presented in detail herein, simulating the annual performance of the combined system in Athens, Copenhagen, Vienna, and Warsaw with an hourly timestep. In this work, the efficiency of two-phase expansion was carefully monitored, by

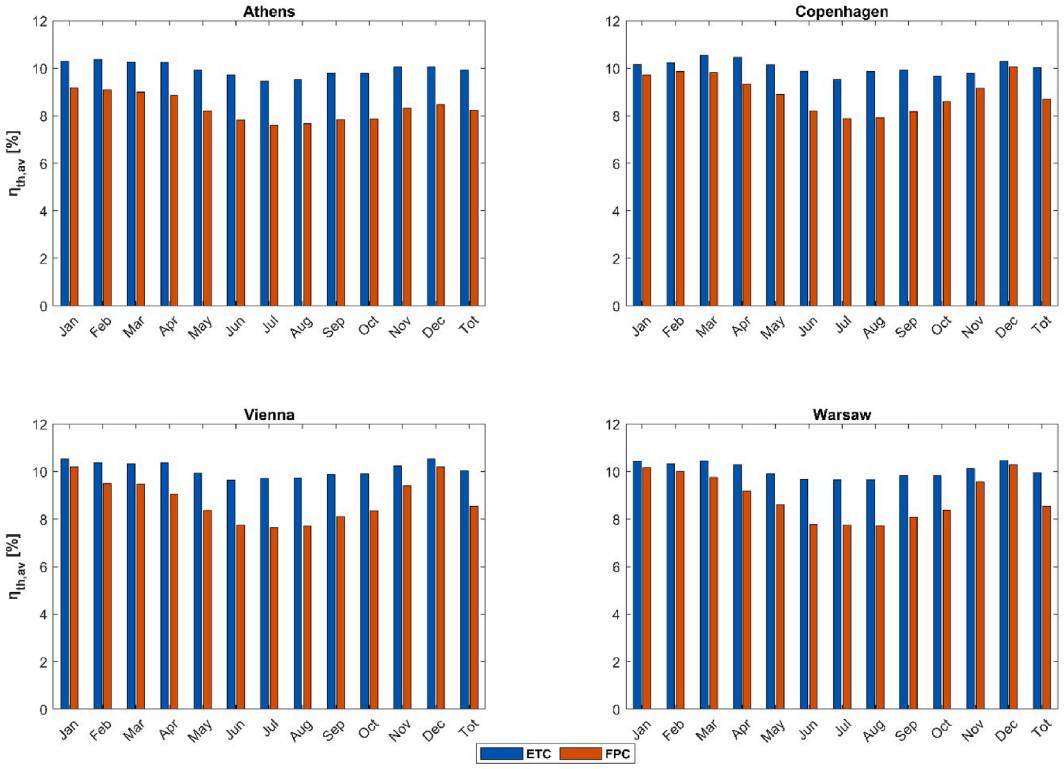

Fig. 9. Monthly and annual $\eta_{th,av}$ of the TFC for the different examined locations and types of solar collectors.

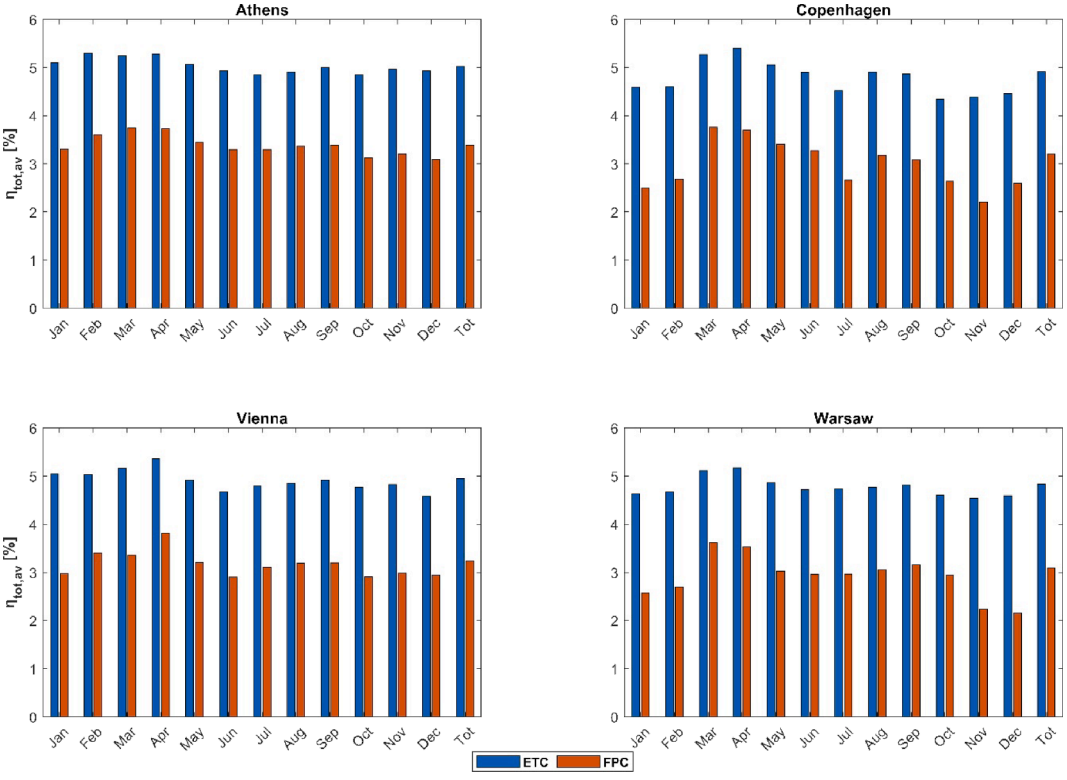

Fig. 10. Monthly and annual $\eta_{tot,av}$ of the Solar-TFC unit for the different examined locations and types of solar collectors.

applying the semi-empirical simulation tool developed by Skiadopoulos et al. [33], because this is the crucial factor affecting the efficiency of the TFC. Two different types of solar collectors, i.e. ETCs and FPCs, were modeled for a more detailed techno-economic analysis.

Following the presentation of the effect of two-phase expansion on the performance of the Solar-TFC unit, a series of numerical experiments aimed at maximizing the total solar energy conversion efficiency in all examined locations was performed. Parameters in the optimization

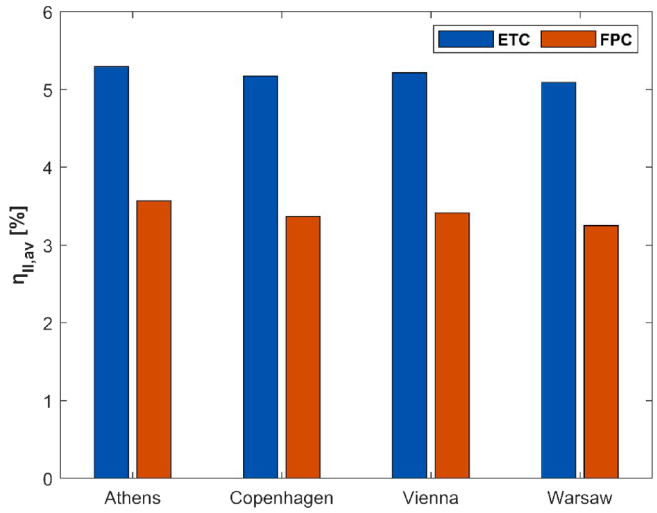

Fig. 11. Annual $\eta_{II,av}$ of the Solar-TFC unit for the different examined locations and types of solar collectors.

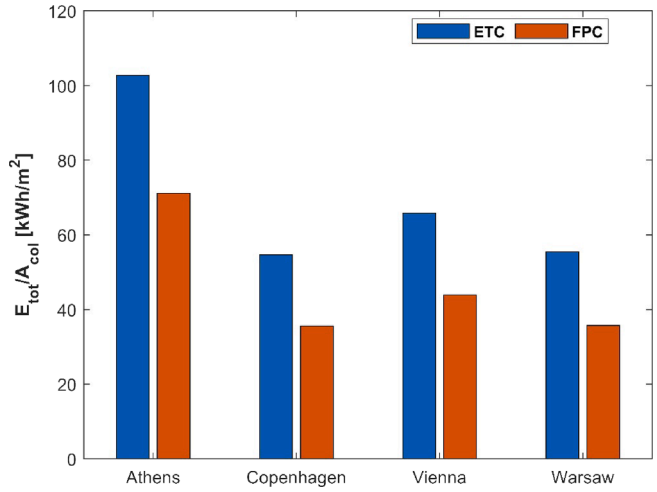

Fig. 12. E_{tot}/A_{col} for the different examined locations and types of solar collectors.

process were the values of T_m and x_3. The ETCs can typically operate at higher T_m than the FPCs because of their inherently increased η_{col} values. However, the optimal T_m is also a function of T_{amb}, because their combination contributes to the determination of the operating pressure ratio of the TFC, and, therefore, to the power output. On the other hand, only increased vapor qualities at the suction port of the expander, between 0.68 and 0.85, can ensure a high $\eta_{ex,is}$, and, therefore, η_{th} and η_{tot}.

Concerning the efficiency of the Solar-TFC, the utilization of ETCs has a positive impact on $\eta_{tot,av}$, $\eta_{th,av}$, and $\eta_{II,av}$. Interestingly, the optimized operation of the Solar-TFC resulted in similar efficiency values for all the examined locations, with a different total electricity output based on the available solar irradiance. $\eta_{tot,av}$, $\eta_{th,av}$, and $\eta_{II,av}$ were estimated approximately equal to 3% and 5 %, 8% and 10 %, and 3.2% and 5.3%, for the FPCs and ETCs, respectively. The value of E_{tot}/A_{col} was estimated between 55 and 103 kWh/m^2 for the ETCs, whereas the respective values for the FPCs were 36 and 71 kWh/m^2. Highest and lowest E_{tot}/A_{col} were in Athens, and Copenhagen, respectively.

The economics of the Solar-TFC were analyzed as a function of A_{col}. As A_{col} increases the economics of the system is improved. Furthermore, the ETCs reduce the *LCOE* because of their increased η_{col} and the significantly higher (45–55%) electricity output compared to the FPCs. When ETCs were modeled, the *LCOE* values were calculated to be between 0.25 and 0.55 €/kWh. On the other hand, for the FPCs, the respective value was in the range between 0.35 and 0.75 €/kWh. The estimated *PBP* highlights the potential competitiveness of the Solar-TFC when ETCs are used. However, an in-depth parametric analysis is necessary to reach a concrete conclusion about the *PBP*.

Finally, concerning the environmental impact of the system, it was concluded that it could be significant not only in regions with high available solar irradiance but also areas with particularly low efficiency of the central power stations and energy transmission systems. Overall, the Solar-TFC unit can reduce the annual GHG emissions by 2.5–47 kg per m^2 of solar collectors, based on the available solar irradiance and the energy efficiency of the centralized power systems. In any case, the utilization of ETCs significantly increases the environmental impact of the Solar-TFC because of the substantially higher electricity output.

CRediT authorship contribution statement

Anastasios Skiadopoulos: Investigation, Conceptualization, Methodology, Software, Formal analysis, Writing – original draft, Writing – review & editing. **Christina Antonopoulou:** Writing – review & editing. **Konstantinos Atsonios:** Project administration, Writing – review & editing. **Panagiotis Grammelis:** Project administration, Funding

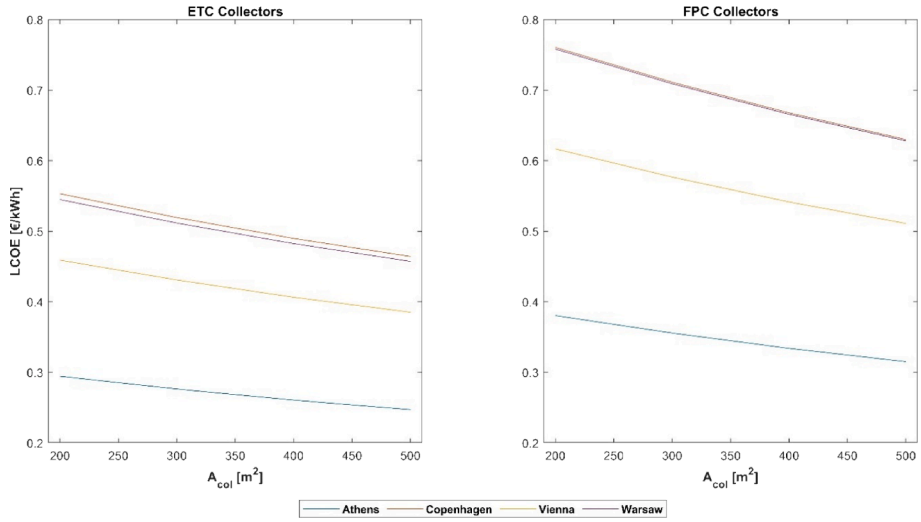

Fig. 13. *LCOE* for the different examined locations and types of solar collectors.

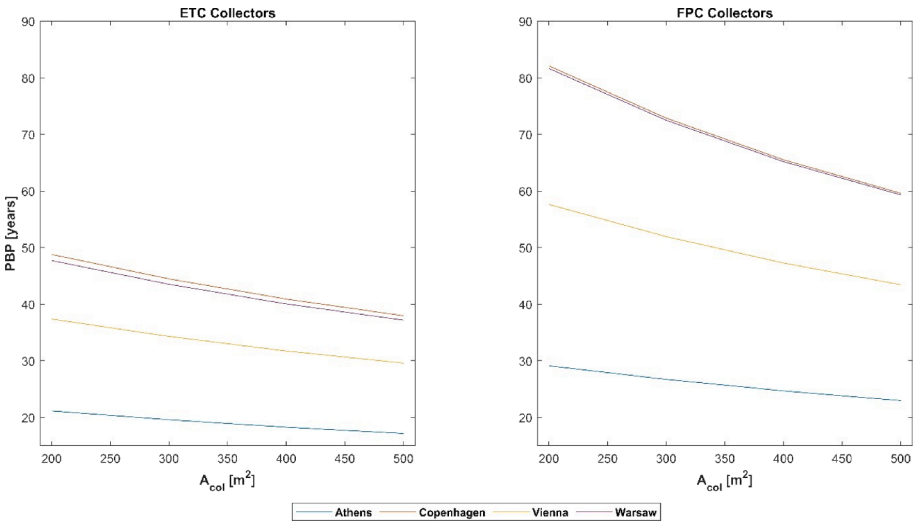

Fig. 14. *PBP* for the different examined locations and types of solar collectors.

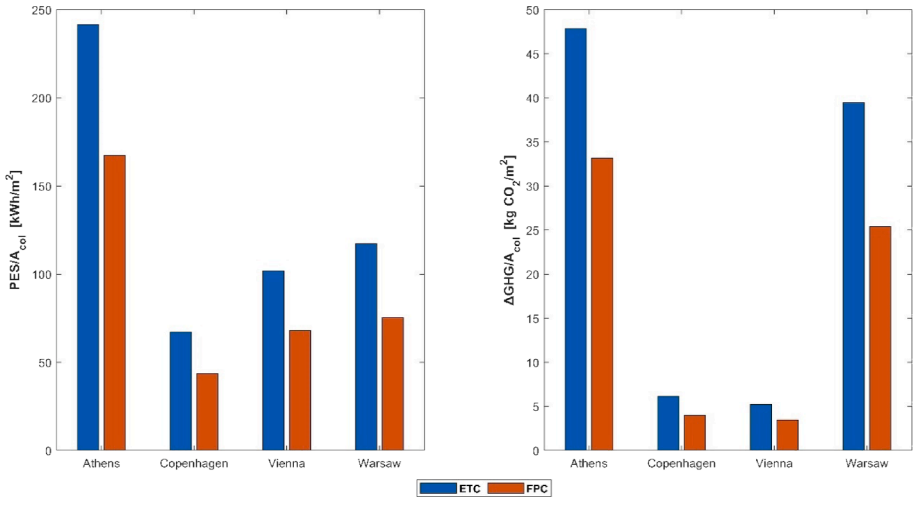

Fig. 15. PES/A_{col} and $\Delta GHG/A_{col}$ for the different examined locations and types of solar collectors.

acquisition. **Apostolos Gkountas:** Writing – review & editing. **Panteleimon Bakalis:** Writing – review & editing. **Dimitrios Manolakos:** Supervision, Project administration, Funding acquisition, Resources.

Declaration of Competing Interest

The authors declare that they have no known competing financial interests or personal relationships that could have appeared to influence the work reported in this paper.

Data availability

The authors do not have permission to share data.

Acknowledgments

This research work was supported by the Operational Programme Competitiveness, Entrepreneurship, and Innovation 2014-2020 (EPAnEK). (Project Number: T2EΔK-00351, Acronym: TRI-MAX).

References

[1] A European Green Deal, (n.d.). https://commission.europa.eu/strategy-and-policy/priorities-2019-2024/european-green-deal_en (accessed February 8, 2023).
[2] EUR-Lex - 52018DC0773 - EN - EUR-Lex, (n.d.). https://eur-lex.europa.eu/legal-content/EN/TXT/?uri=CELEX:52018DC0773 (accessed May 15, 2023).
[3] Kalogirou SA. Solar thermal collectors and applications. Prog Energy Combust Sci 2004;30:231–95. https://doi.org/10.1016/J.PECS.2004.02.001.
[4] Karellas S, Roumpedakis TC. Solar thermal power plants. Solar Hydrogen Prod: Process Syst Technol 2019:179–235. https://doi.org/10.1016/B978-0-12-814853-2.00007-2.
[5] Markides CN. Low-concentration solar-power systems based on organic rankine cycles for distributed-scale applications: Overview and further developments. Front Energy Res 2015;3:47. https://doi.org/10.3389/FENRG.2015.00047/BIBTEX.
[6] Morais PHdS, Lodi A, Aoki AC, Modesto M. Energy, exergetic and economic analyses of a combined solar-biomass-ORC cooling cogeneration systems for a Brazilian small plant. Renew Energy 2020;157:1131–47.
[7] Papingiotis T, Koronaki I, Komninos N, Antonakos G. Thermodynamic analysis and optimization of Transcritical and Supercritical Organic Rankine and Brayton Cycles coupled to parabolic trough collectors. IOP Conf Ser Mater Sci Eng 2021;1037. https://doi.org/10.1088/1757-899X/1037/1/012044.
[8] Tchanche BF, Lambrinos G, Frangoudakis A, Papadakis G. Low-grade heat conversion into power using organic Rankine cycles – A review of various applications. Renew Sustain Energy Rev 2011;15:3963–79. https://doi.org/10.1016/J.RSER.2011.07.024.
[9] Lecompte S, Huisseune H, van den Broek M, De Paepe M. Methodical thermodynamic analysis and regression models of organic Rankine cycle architectures for waste heat recovery. Energy 2015;87:60–76. https://doi.org/10.1016/j.energy.2015.04.094.

[10] Tareq Chowdhury M, Mokheimer EMA. Recent developments in solar and low-temperature heat sources assisted power and cooling systems: A design perspective. J Energy Resour Technol Trans ASME 2020;142. https://doi.org/10.1115/1.4044562.
[11] Golonis C, Skiadopoulos A, Manolakos D, Kosmadakis G. Assessment of the performance of a low-temperature Organic Rankine Cycle engine coupled with a concentrating PV-Thermal system. Renew Energy 2021;179:1085–97. https://doi.org/10.1016/J.RENENE.2021.07.103.
[12] Manolakos D, Kosmadakis G, Kyritsis S, Papadakis G. Identification of behaviour and evaluation of performance of small scale, low-temperature Organic Rankine Cycle system coupled with a RO desalination unit. Energy 2009;34:767–74. https://doi.org/10.1016/J.ENERGY.2009.02.008.
[13] Heberle F, Schifflechner C, Brüggemann D. Life cycle assessment of Organic Rankine Cycles for geothermal power generation considering low-GWP working fluids. Geothermics 2016;64:392–400. https://doi.org/10.1016/J.GEOTHERMICS.2016.06.010.
[14] Kalina J, Świerzewski M. Identification of ORC unit operation in biomass-fired cogeneration system. Renew Energy 2019;142:400–14. https://doi.org/10.1016/J.RENENE.2019.04.080.
[15] Delgado-Torres AM, García-Rodríguez L. Analysis and optimization of the low-temperature solar organic Rankine cycle (ORC). Energy Convers Manag 2010;51:2846–56. https://doi.org/10.1016/J.ENCONMAN.2010.06.022.
[16] Soulis KX, Manolakos D, Ntavou E, Kosmadakis G. A geospatial analysis approach for the operational assessment of solar ORC systems. Case study: Performance evaluation of a two-stage solar ORC engine in Greece. Renew Energy 2022;181:116–28. https://doi.org/10.1016/J.RENENE.2021.09.046.
[17] Roumpedakis TC, Loumpardis G, Monokrousou E, Braimakis K, Charalampidis A, Karellas S. Exergetic and economic analysis of a solar driven small scale ORC. Renew Energy 2020;157:1008–24. https://doi.org/10.1016/J.RENENE.2020.05.016.
[18] Lai NA, Fischer J. Efficiencies of power flash cycles. Energy 2012;44:1017–27. https://doi.org/10.1016/J.ENERGY.2012.04.046.
[19] Fischer J. Comparison of trilateral cycles and organic Rankine cycles. Energy 2011;36:6208–19. https://doi.org/10.1016/J.ENERGY.2011.07.041.
[20] Schuster A, Karellas S, Aumann R. Efficiency optimization potential in supercritical Organic Rankine Cycles. Energy 2010;35:1033–9. https://doi.org/10.1016/J.ENERGY.2009.06.019.
[21] DiPippo R. Ideal thermal efficiency for geothermal binary plants. Geothermics 2007;36:276–85. https://doi.org/10.1016/J.GEOTHERMICS.2007.03.002.
[22] Smith IK. Development of the Trilateral Flash Cycle System: Part 1: Fundamental Considerations. Proc Inst Mech Eng, Part A: J Power Energy 1993;207(3):179–94.
[23] Lecompte S, van den Broek M, De Paepe M, Thermodynamic analysis of the partially evaporating trilateral cycle. In: 2nd International Seminar on ORC Power Systems, Proceedings. http://hdl.handle.net/1854/LU-4166776 (accessed February 9, 2023): 2013.
[24] Iqbal MA, Rana S, Ahmadi M, Date A, Akbarzadeh A. Trilateral flash cycle (TFC) a promising thermodynamic cycle for low grade heat to power generation. Energy Procedia 2019;160:208–14. https://doi.org/10.1016/J.EGYPRO.2019.02.138.
[25] Daniarta S, Kolasiński P, Imre AR. Thermodynamic efficiency of trilateral flash cycle, organic Rankine cycle and partially evaporated organic Rankine cycle. Energy Convers Manag 2021;249. https://doi.org/10.1016/J.ENCONMAN.2021.114731.
[26] Kanno H, Shikazono N. Experimental study on two-phase adiabatic expansion in a reciprocating expander with intake and exhaust processes. Int J Heat Mass Transf 2016;102:1004–11. https://doi.org/10.1016/j.ijheatmasstransfer.2016.06.081.
[27] Smith IK, Stošić N, Aldis CA, Development of the trilateral flash cycle system. Part 3: The design of high-efficiency two-phase screw expanders. Proc Inst Mech Eng, Part A: J Power Energy. 1996;210:75–92. 10.1243/pime_proc_1996_210_010_02.
[28] Öhman H, Lundqvist P. Experimental investigation of a Lysholm Turbine operating with superheated, saturated and 2-phase inlet conditions. Appl Therm Eng 2013;50(1):1211–8.
[29] Dawo F, Buhr J, Schifflechner C, Wieland C, Spliethoff H. Experimental assessment of an Organic Rankine Cycle with a partially evaporated working fluid. Appl Therm Eng 2023;221:119858. https://doi.org/10.1016/J.APPLTHERMALENG.2022.119858.
[30] Bianchi G, Kennedy S, Zaher O, Tassou SA, Miller J, Jouhara H. Numerical modeling of a two-phase twin-screw expander for Trilateral Flash Cycle applications. Int J Refrig 2018;88:248–59. https://doi.org/10.1016/J.IJREFRIG.2018.02.001.
[31] Vasuthevan H, Brümmer A. Theoretical investigation of flash vaporisation in a screw expander. IOP Conf Ser: Mater Sci Eng 2017;232:012077.
[32] Taniguchi H, Kudo K, Giedt WH, Park I, Kumazawa S. Analytical and experimental investigation of two-phase flow screw expanders for power generation. J Eng Gas Turbine Power 1988;110:628–35. https://doi.org/10.1115/1.3240182.
[33] Skiadopoulos A, van Heule X, Kosmadakis G, Manolakos D, de Paepe M, Lecompte S, Thermodynamic low-order model for the simulation of two-phase expansion within a TFC unit. In: T.U. of Munich (Ed.), Proceedings of the 6th International Seminar on ORC Power Systems, Technical University of Munich, 2021.
[34] JRC Photovoltaic Geographical Information System (PVGIS) - European Commission, (n.d.). https://re.jrc.ec.europa.eu/pvg_tools/en/#PVP (accessed May 17, 2023).
[35] Kingspan Solar Thermal/Thermomax - The Small Solar Company, (n.d.). https://www.smallsolar.co.uk/solar-panel-manufacturers/kingspan-solar-thermomax/ (accessed May 18, 2023).
[36] Klimalösungen: Effizient heizen, kühlen, lüften | Viessmann LU, (n.d.). https://www.viessmann.lu/de.html (accessed May 18, 2023).
[37] Thermomax DF 100-30- Datasheet, (n.d.). https://tinyurl.com/2p9z8kxt (accessed July 28, 2023).
[38] Vitosol 300-F- Datasheet, (n.d.). https://tinyurl.com/3dpk8mf5 (accessed July 28, 2023).
[39] Kalogirou SA, Solar energy engineering: Processes and systems, Solar Energy Engineering: Processes and Systems. 2009:1–760. 10.1016/B978-0-12-374501-9.X0001-5.
[40] Bell IH, Wronski J, Quoilin S, Lemort V. Pure and pseudo-pure fluid thermophysical property evaluation and the open-source thermophysical property library coolprop. Ind Eng Chem Res 2014;53:2498–508. https://doi.org/10.1021/IE4033999/SUPPL_FILE/IE4033999_SI_002.ZIP.
[41] Balaji K, Iniyan S, Swami MV. Exergy, economic and environmental analysis of forced circulation flat plate solar collector using heat transfer enhancer in riser tube. J Clean Prod 2018;171:1118–27. https://doi.org/10.1016/J.JCLEPRO.2017.10.093.
[42] Braimakis K, Karellas S. Integrated thermoeconomic optimization of standard and regenerative ORC for different heat source types and capacities. Energy 2017;121:570–98. https://doi.org/10.1016/J.ENERGY.2017.01.042.
[43] Efficiency of conventional thermal electricity and heat production in Europe — European Environment Agency, (n.d.). https://www.eea.europa.eu/data-and-maps/indicators/efficiency-of-conventional-thermal-electricity-generation-4/assessment-2 (accessed May 19, 2023).
[44] Greenhouse gas emission intensity of electricity generation — European Environment Agency, (n.d.). https://www.eea.europa.eu/data-and-maps/daviz/co2-emission-intensity-12#tab-googlechartid_chart_11 (accessed May 19, 2023).